Spatially resolved spin angular momentum mediated by spin-orbit interaction in tightly focused spinless vector beams in optical tweezers: Supplementary Information

Ram Nandan Kumar[a†], Sauvik Roy[a], Subhasish Dutta Gupta[a,b,c], Nirmalya Ghosh[a*], Ayan Banerjee[a*†]

[a]Indian Institute of Science Education and Research Kolkata, Department of Physical Sciences, Mohanpur-741246, West Bengal, India

[b]Tata Institute of Fundamental Research, Hyderabad, Telangana 500046, India

[c]Indian Institute of Technology, Department of Physics, Jodhpur 342030, India

† rnk17ip025@iiserkol.ac.in, * nghosh@iiserkol.ac.in, *† ayan@iiserkol.ac.in

1 Theoretical calculations

The study of spin-orbit interaction (SOI) of light in the non-paraxial regime (particularly in optical tweezers) requires a robust theoretical framework to accurately describe the behavior of light as it propagates and interacts with stratified media of varying refractive indices and anisotropic media containing birefringent particles. The Debye-Wolf theory or the angular spectrum method provides prominent approaches to analyzing the SOI of light in this regime. The Debye-Wolf-based angular spectrum method operates in the frequency domain and involves decomposing an incoming collimated structured beam into a superposition of plane waves, each associated with a distinct spatial harmonic component (k-vector). Before focusing, the collimated beam exhibits cylindrical symmetry; however, after passing through an aplanatic lens or a high numerical aperture (NA) objective lens, the beam assumes spherical symmetry. The Debye-Wolf formalism then begins by calculating the Fourier transform (FT) of the input field E_{inc}, which is subsequently multiplied by the lens's transfer function to account for the transformation from cylindrical to spherical coordinates. The resulting output field E_{res} (or $E_{\infty}(\theta, \phi)$) is obtained by taking the inverse FT. The focused field is ultimately determined by the linear superposition of the TE (s-polarization) and

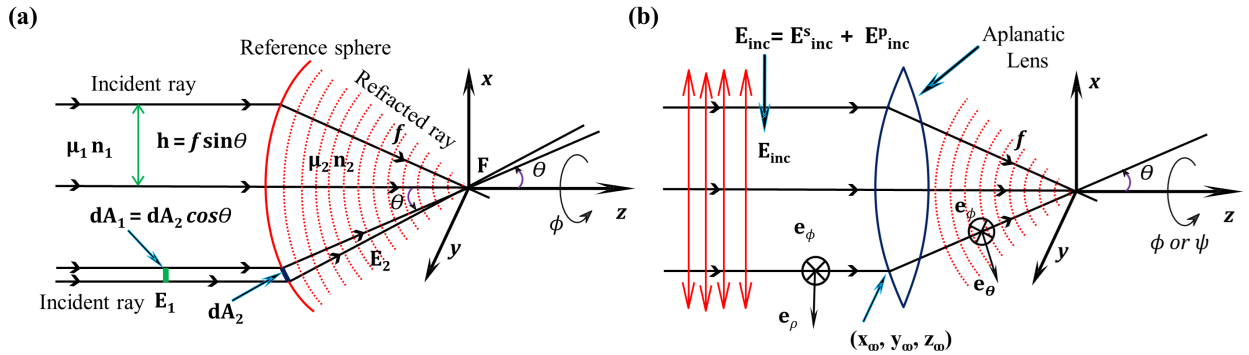

Fig 1 (a) Illustration of the sine condition and intensity law in geometrical optics. The refracted ray and its corresponding incident ray intersect at the surface of the reference sphere (or aplanatic lens), with the energy flux carried by each ray remaining constant before and after focusing through the aplanatic lens. (b) Geometric representation of the transformation from cylindrical to spherical coordinates through the aplanatic system.

TM (p-polarization) components of all plane waves, thus retaining the full vectorial nature of the field in the image plane.[1–3]

1.1 The Debye-Wolf or Angular spectrum representation

The Debye-Wolf based angular spectrum integral of the focused field can be expressed as:[1–3]

$$E(\rho,\psi,z) = \frac{\mathrm{i}kf\mathrm{e}^{-\mathrm{i}kf}}{2\pi}\int_0^{\theta_{\max}}\int_0^{2\pi} E_\infty(\theta,\phi)\mathrm{e}^{\mathrm{i}kz\cos\theta}\mathrm{e}^{\mathrm{i}k\rho\sin\theta\cos(\phi-\psi)}\sin\theta\mathrm{d}\phi\mathrm{d}\theta. \tag{1}$$

This integral determines the electric field at the focal plane (or image plane) of a collimated beam focused through an aplanatic lens or a high numerical aperture (NA) objective lens. Here, we neglect the evanescent fields and consider only the far-field component, denoted as $E_\infty(\theta,\phi)$. The term $E_\infty(\theta,\phi)$ represents the field at $r = (x^2+y^2+z^2)^{1/2} \to \infty$ (where r is the distance from the origin). We assume that the fields at r_∞ and at the reference sphere (or the aplanatic lens) are equivalent because the incoming beam is assumed to be paraxially collimated. Therefore, the distance r_∞ between the focal point and the surface of the reference sphere can be replaced by the focal length of the lens, f.

To calculate the $E_\infty(\theta, \phi)$ component of Eq. 1 for the ARP vector beam, we first need to describe the function of an aplanatic lens and the coordinate transformation through it. This requires two fundamental principles: (1) the sine condition and (2) the intensity law.

(1) The sine condition:- This condition states that every optical ray either emerging from or converging to the focal point F of an aplanatic optical system intersects its corresponding conjugate ray on a reference sphere with radius f, where f is the focal length of the lens (or the radius of curvature of reference sphere). The distance h from the optical axis to the conjugate ray is given by $h = f \times \sin\theta$, where θ is the divergence angle of the conjugate ray, as illustrated in Figure 1 (a).

(2) The intensity law:- This law is based on the energy conservation principle: it ensures that the energy entering the aplanatic lens is equal to the energy exiting the lens. Mathematically, the power carried by a ray can be expressed as $P = \frac{1}{2} Z_{\mu\varepsilon}^{-1/2} |E|^2 \mathrm{d}A$, where $Z_{\mu\varepsilon}$ is the wave impedance, and $\mathrm{d}A$ is an infinitesimal cross-sectional area perpendicular to the ray's direction. As a result, the fields before and after refraction must satisfy the condition that the energy flux carried by each ray remains constant, as shown in Figure 1 (a).

$$|E_2| = |E_1| \sqrt{\frac{n_1}{n_2}} \sqrt{\frac{\mu_2}{\mu_1}} \cos^{1/2}\theta \tag{2}$$

For a non-magnetic medium, the magnetic permeability (μ) at optical frequencies is equal to one ($\mu = 1$). Thus, Eq.2 simplifies to:

$$|E_2| = |E_1| \sqrt{\frac{n_1}{n_2}} \cos^{1/2}\theta \tag{3}$$

According to the sine condition, the incident light ray and the refracted ray intersect at a point on the reference sphere with a radius of f. This intersection point on the surface of the reference sphere is denoted by $(x_\infty, y_\infty, z_\infty)$, while an arbitrary field point near the focus is represented by $(x, y, z) = (0, 0, 0)$, as shown in Figure 1 (b). These two points can also be expressed in spherical coordinates as (f, θ, ϕ) and (ρ, ϑ, ψ), respectively.

The aplanatic lens (or reference sphere) effectively transforms the cylindrical coordinate system (associated with the incoming beam) into a spherical coordinate system (associated with the focused beam). To describe the refraction of the incident rays at the reference sphere, as shown in Fig. 1 (b), we introduce the unit vectors $\mathbf{e}_\rho$, $\mathbf{e}_\phi$, and $\mathbf{e}_\theta$. Here, $\mathbf{e}_\rho$ and $\mathbf{e}_\phi$ are the unit vectors in the cylindrical coordinate system, while $\mathbf{e}_\theta$ and $\mathbf{e}_\phi$ are the unit vectors in the spherical coordinate system. During the coordinate transformation, only $\mathbf{e}_\rho$ transforms into $\mathbf{e}_\theta$, while the unit vector $\mathbf{e}_\phi$ remains unaffected, as shown in Fig. 1 (b).

Considering the more general case where the incoming collimated beam has arbitrary homogeneous or inhomogeneous polarization distributions, any arbitrarily polarized field can be expressed in terms of the s and p orthogonal polarization bases as $E_{inc} = E^s_{inc} + E^p_{inc}$. Consequently, we can easily calculate the refraction at the reference sphere by decomposing the incident field E_{inc} into its two components: $E^{(s)}_{inc}$ and $E^{(p)}_{inc}$, where the indices (s) and (p) denote s-polarization and p-polarization, respectively. These two fields can then be expressed using the corresponding unit vectors as follows:

$$E^{(s)}_{inc} = [E_{\text{inc}} \cdot \mathbf{e}_\phi]\, \mathbf{e}_\phi \;\; ; \;\; E^{(p)}_{inc} = [E_{\text{inc}} \cdot \mathbf{e}_\rho]\, \mathbf{e}_\rho \tag{4}$$

As shown in Fig. 1 (b), these two fields refract at the spherical surface differently. Thus, the

total refracted electric field, denoted by $E_\infty(\theta,\phi)$, can be expressed as

$$E_\infty(\theta,\phi) = \left[t^{\mathrm{s}}\left(E_{\mathrm{inc}}\cdot\mathbf{e}_\phi\right)\mathbf{e}_\phi + t^{\mathrm{p}}\left(E_{\mathrm{inc}}\cdot\mathbf{e}_\rho\right)\mathbf{e}_\theta\right]\sqrt{\frac{n_1}{n_2}}(\cos\theta)^{1/2} \tag{5}$$

Here, t^s and t^p are the Fresnel transmission coefficients for each refracted ray passing through the aplanatic lens, and $\cdot$ represents the dot (scalar) product between the incident polarized field and the corresponding cylindrical unit vector. The factor outside the brackets, $\sqrt{\frac{n_1}{n_2}}(\cos\theta)^{1/2}$, arises from the intensity law to ensure energy conservation, where n_1 and n_2 are the refractive indices of the medium before and after focusing through an aplanatic lens (or reference sphere), respectively. To conveniently handle the focused field in the Cartesian coordinate system, we need to express the cylindrical and spherical unit vectors $\mathbf{e}_\rho$, $\mathbf{e}_\phi$, and $\mathbf{e}_\theta$ in terms of the Cartesian unit vectors $\mathbf{e}_x$, $\mathbf{e}_y$, and $\mathbf{e}_z$, as shown in Fig. 1 (b). This transformation can be achieved using the following matrix:

$$\begin{bmatrix}\mathbf{e}_\rho\\ \mathbf{e}_\phi\\ \mathbf{e}_\theta\end{bmatrix} = \begin{bmatrix}\cos\phi & \sin\phi & 0\\ -\sin\phi & \cos\phi & 0\\ \cos\theta\cos\phi & \cos\theta\sin\phi & -\sin\theta\end{bmatrix}\begin{bmatrix}\mathbf{e}_x\\ \mathbf{e}_y\\ \mathbf{e}_z\end{bmatrix} \tag{6}$$

1.2 Focal fields of spirally polarized vector (SPV) beam

We assume the incoming beam is paraxially collimated and have an anti-clockwise or clockwise spiral polarization distribution and doughnut intensity profile. Therefore, we can write the incident ARP doughnut vector mode ($E_{inc} = E_{inc}(\theta,\phi)\left(\mathbf{e}_\rho \pm \mathbf{e}_\phi\right)$) as[4,5]

$$E_{\mathrm{inc}}^{SPV}(\rho,\phi,z) = (E_0/w_0)\,\rho\exp\left(-\frac{\rho^2}{w^2}\right)\begin{pmatrix}\cos\phi \pm \sin\phi\\ \sin\phi \mp \cos\phi\end{pmatrix}, \tag{7}$$

Here, E_0 is the overall amplitude factor, and w_0 is the size of the paraxially collimated beam before focusing. The focal field $E(\rho, \psi, z)$ depends on how much the incoming beam is spatially expanded relative to the lens size. Since the aperture radius of the aplanatic lens is $f \sin\theta_{\text{max}}$, as shown in Fig. 1 (a), we introduce the filling factor f_0 as $f_0 = \frac{w_0}{f \sin\theta_{\text{max}}}$, where $\theta_{\text{max}} = \sin^{-1}(\text{NA}/n)$ is the maximum angle determined by the numerical aperture (NA) of the objective lens, and n denotes the refractive index of the medium. Hence, the function $f_\omega(\theta) = \mathrm{e}^{-\frac{1}{f_0^2}\frac{\sin^2\theta}{\sin^2\theta_{\text{max}}}}$ is the apodization function that arises when an aplanatic lens tightly focuses the beam.[1,2,6] Therefore we can write equation 7 in terms of the apodization function in spherical coordinates as

$$E_{\text{inc}}^{SPV}(\theta, \phi) = (E_0 f / w_0) \sin\theta \; f_\omega(\theta) \begin{pmatrix} \cos\phi \pm \sin\phi \\ \\ \sin\phi \mp \cos\phi \end{pmatrix} \tag{8}$$

The back aperture of an aplanatic lens (or microscope objective) typically has a diameter of about 4.5 mm. To fully utilize the objective lens, the incident field should either fill or slightly overfill this aperture. We assume that the waist of the paraxially collimated beam is aligned with the lens and that it strikes the lens with a planar phase front. However, since no lens is ideal, it will always reflect some portion of the incident light. We assume the objective lens has an effective anti-reflection coating, allowing us to set the Fresnel transmission coefficients, t^s and t^p, equal to 1. However, the focused light from the microscope objective also passes through a stratified medium with varying refractive indices, as shown in Figure 1 (a) in the main manuscript (ms). Therefore, we consider the more general case where the Fresnel transmission coefficients, t^s and t^p, and reflection coefficients, r^s and r^p, are not equal to 1. Based on these assumptions and using Eqs. 6 and 8, we can express Eq. 5, $E_\infty^{SPV}(\theta, \phi)$, as

$$E_{\infty}^{SPV}(\theta,\phi) = (E_0 f/\omega_0)\ f_{\omega}(\theta)\ \sqrt{\frac{n_1}{n_2}}(\cos\theta)^{1/2}\ \sin\theta \begin{bmatrix} t^p\cos\theta\ \cos\phi \pm t^s\ \sin\phi \\ t^p\cos\theta\ \sin\phi \mp t^s\ \cos\phi \\ -\ t^p\sin\theta \end{bmatrix} \tag{9}$$

It is important to note that, in general, $E_{\infty}(\theta,\phi)$ represents a superposition of both forward- and backwards-propagating waves in the stratified medium. We evaluate Eqs. 9 only for the forward-propagating waves, as they provide the dominant contribution. However, these equations can also be expressed for the backwards-propagating waves by modifying the θ-dependent coefficients t^s and t^p. This is done by replacing θ with $\pi - \theta$. Additionally, the Fresnel reflection coefficients r^s and r^p are used instead of the transmission coefficients in this case.[3,7]

We use the mathematical relations provided in Eq.10 below to analytically calculate the angular spectrum integration over ϕ in Eq.1.[2,8]

$$\begin{aligned}
&\int_0^{2\pi} e^{ik\rho\sin\theta\cdot\cos(\phi-\psi)}d\phi = 2\pi\ J_0(k\rho\sin\theta), \\
&\int_0^{2\pi} \cos\phi e^{ik\rho\sin\theta\cdot\cos(\phi-\psi)}d\phi = 2\pi\ iJ_1(k\rho\sin\theta)\cos\psi, \\
&\int_0^{2\pi} \sin\phi e^{ik\rho\sin\theta\cdot\cos(\phi-\psi)}d\phi = 2\pi\ iJ_1(k\rho\sin\theta)\sin\psi
\end{aligned} \tag{10}$$

Here, J_0 and J_1 are the zeroth and first-order Bessel functions of the first kind, respectively. Using equations 1, 9, and 10, we proceed as follows: First, we substitute the value of $E_{\infty}^{\text{SPV}}(\theta,\phi)$ from Eq. 9 into Eq. 1. Then, we evaluate the integral over ϕ separately using Eq. 10 and substitute it back into Eq. 1. Consequently, the final expressions for the focal field in Eq. 1 now involve a single integration over the variable θ, which can be expressed in terms of the Debye–Wolf (or

diffraction) integrals as follows:

$$\begin{bmatrix} E_x \\ E_y \\ E_z \end{bmatrix}_{\text{SPV}}^{\text{ACW/CW}} = \begin{bmatrix} i\left(I_1 \cos\psi \pm I_2 \sin\psi\right) \\ i\left(I_1 \sin\psi \mp I_2 \cos\psi\right) \\ -I_0 \end{bmatrix} \tag{11}$$

Similarly, we can calculate the magnetic field in terms of Debye–Wolf (or diffraction) integrals as follows:

$$\begin{bmatrix} H_x \\ H_y \\ H_z \end{bmatrix}_{\text{SPV}}^{\text{ACW/CW}} = \begin{bmatrix} \pm i\left(I_1 \cos\psi \mp I_2 \sin\psi\right) \\ \pm i\left(I_1 \sin\psi \pm I_2 \cos\psi\right) \\ \mp I_0 \end{bmatrix} \tag{12}$$

Where $\vec{E}_{\text{SPV}}^{\text{ACW/CW}} = \boldsymbol{E}_{\text{rad}} \pm \boldsymbol{E}_{\text{azi}}$ and $\vec{H}_{\text{SPV}}^{\text{ACW/CW}} = \boldsymbol{H}_{\text{rad}} \pm \boldsymbol{H}_{\text{azi}}$ are the electric and magnetic fields of the focused light, respectively. The subscript "SPV" represents the spirally polarized vector (SPV) beam, while the superscripts "ACW" and "CW" denote the anti-clockwise and clockwise spiral polarization directions, respectively. It is important to note that the magnetic field is CW in nature for the input ACW-SPV beam; however, it is ACW in nature for the input CW-SPV beam, with equal and opposite non-zero z-components in both cases. The diffraction integrals for the transmitted and reflected waves, $I_0 = I_0^t(\rho) + I_0^r(\rho)$, $I_1 = I_1^t(\rho) + I_1^r(\rho)$ and $I_2 = I_2^t(\rho) + I_2^r(\rho)$, are determined by the polar angles of incidence (θ) of the plane waves, and by Fresnel's transmission (t^s, t^p) and reflection (r^s, r^p) coefficients. These integrals encapsulate the strength of the spin-orbit

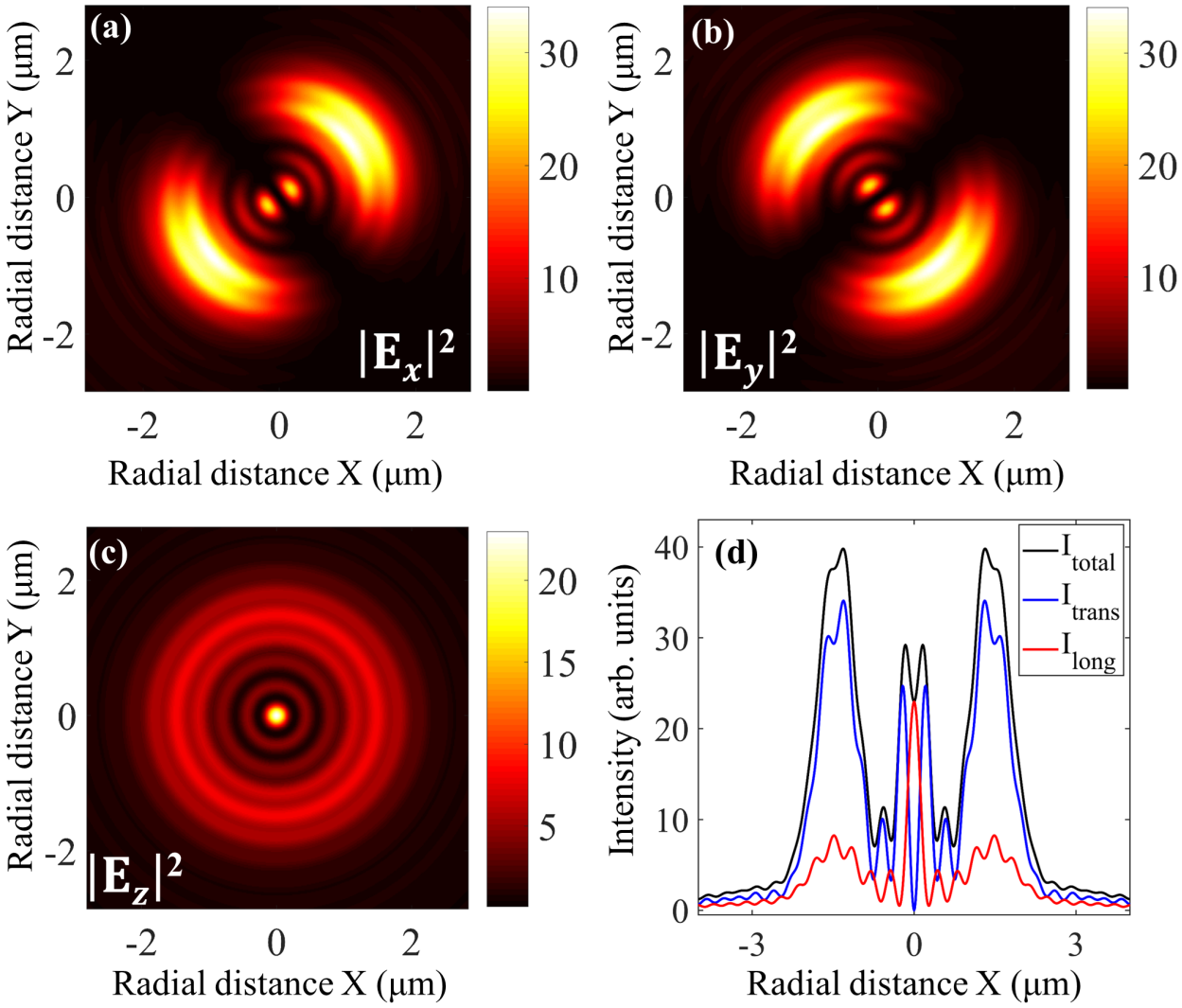

Fig 2 Numerical simulations of the squared magnitudes of the electric field components: (a) $|E_x|^2$, (b) $|E_y|^2$, and (c) $|E_z|^2$ at a distance of $z = 2, \mu$m from the focus for a refractive index (RI) of 1.814, using a high numerical aperture (NA) objective lens. (d) Comparison of the electric field intensities of the transverse and longitudinal components relative to the total field intensity (transverse + longitudinal) at both off-axis and on-axis (beam center) positions in the transverse plane.

conversion, which are given as:[2,3,9,10]

$$
\begin{aligned}
I_1^t(\rho) &= \int_0^{\theta_{\max}} f_\omega(\theta)\,\sqrt{\cos\theta}\,\sin^2\theta\,\left(t^p_{(1,\,j)}\cos\theta_j\right)\,J_1\left(k_1\rho\sin\theta\right)\,e^{ik_jz\cos\theta_j}\,d\theta,\\
I_2^t(\rho) &= \int_0^{\theta_{\max}} f_\omega(\theta)\,\sqrt{\cos\theta}\,\sin^2\theta\,\left(t^s_{(1,\,j)}\right)\,J_1\left(k_1\rho\sin\theta\right)\,e^{ik_jz\cos\theta_j}\,d\theta,\\
I_0^t(\rho) &= \int_0^{\theta_{\max}} f_\omega(\theta)\,\sqrt{\cos\theta}\,\sin^2\theta\,\left(t^p_{(1,\,j)}\sin\theta_j\right)\,J_0\left(k_1\rho\sin\theta\right)\,e^{ik_jz\cos\theta_j}\,d\theta,\\
I_1^r(\rho) &= \int_0^{\theta_{\max}} f_\omega(\theta)\,\sqrt{\cos\theta}\,\sin^2\theta\,\left(-r^p_{(1,\,j)}\cos\theta_j\right)\,J_1\left(k_1\rho\sin\theta\right)\,e^{-ik_jz\cos\theta_j}\,d\theta,\\
I_2^r(\rho) &= \int_0^{\theta_{\max}} f_\omega(\theta)\,\sqrt{\cos\theta}\,\sin^2\theta\,\left(r^s_{(1,\,j)}\right)\,J_1\left(k_1\rho\sin\theta\right)\,e^{-ik_jz\cos\theta_j}\,d\theta,\\
I_0^r(\rho) &= \int_0^{\theta_{\max}} f_\omega(\theta)\,\sqrt{\cos\theta}\,\sin^2\theta\,\left(r^p_{(1,\,j)}\sin\theta_j\right)\,J_0\left(k_1\rho\sin\theta\right)\,e^{-ik_jz\cos\theta_j}\,d\theta,
\end{aligned}
\tag{13}
$$

The superscripts t and r indicate the transmitted and reflected components, respectively. The subscript j specifies the layer of the stratified medium where the trapping laser of the optical tweezers is focused.

2 Numerical Simulations

Our simulations focus on the tight focusing of the input ACW-SPV/CW-SPV beam through a high NA objective lens into a stratified medium, as described in the main manuscript. The electric and magnetic fields of the SPV beam in the focal plane exhibit components not only in the transverse direction but also in the longitudinal direction, due to the fact that the zero-order Bessel function of the first kind, J_0, is non-zero at the beam's focus. As mentioned in the main manuscript, the transverse components of the electric field are governed by the Debye–Wolf integrals I_1 and I_2, which involve the 1^{st}-order Bessel function J_1, while the longitudinal component is determined by I_0, which involves the 0^{th}-order Bessel function J_0. In Figs. 2 (a) and (b), the intensity lobes corresponding to the x and y components of the electric field ($|E_x|^2$ and $|E_y|^2$) are oriented at 45°

and -45° (or 135°), respectively. The intensity lobe patterns arise from the linear combination of $\cos\psi$ and $\sin\psi$ in the expressions for E_x and E_y (see Eq. 11). However, the intensity corresponding to the z component of the electric field ($|E_z|^2$) forms a concentric ring, as shown in Fig. 2 (c). In Fig. 2 (d), the comparison of the electric field intensities of the transverse and longitudinal components relative to the total field intensity (transverse + longitudinal) is shown for both off-axis and on-axis (beam center) positions in the transverse plane. The intensity corresponding to the longitudinal component of the electric field is mostly concentrated at the beam center and less distributed at the off-axis position. In contrast, the intensity corresponding to the transverse component of the electric field is predominantly concentrated at the off-axis position and less distributed near the beam center.

*2.1 **Comparison of LSAM distributions before and after the focus***

The characteristics of LSAM distributions before and after the focus exhibit distinct differences. In Fig. 3(c), we plotted the LSAM distribution at the focus and observed that, for an input anti-clockwise spirally polarized vector (ACW-SPV) beam, the spatially resolved LSAM distribution closer to the beam center (i.e., the first annular ring of LSAM) is positive ($\sigma = +1$), while the second consecutive annular ring is negative ($\sigma = -1$). For an input clockwise spirally polarized vector (CW-SPV) beam, the distribution pattern of LSAM remains the same, but the signs of $\sigma = +1$ and $\sigma = -1$ are reversed. Beyond the focus (i.e., for positive values of z), the same LSAM distribution characteristics persist, as shown in Figs.3(d) and (f).

However, before the focus, the separation of $\sigma = +1$ and $\sigma = -1$ helicities occurs not only in the transverse plane but also along the axial direction (z-axis), as illustrated in Figs. 3(a), (b), and (e). For an input ACW-SPV beam, at the focus and at $z = -2\,\mu$m before the focus, the first and

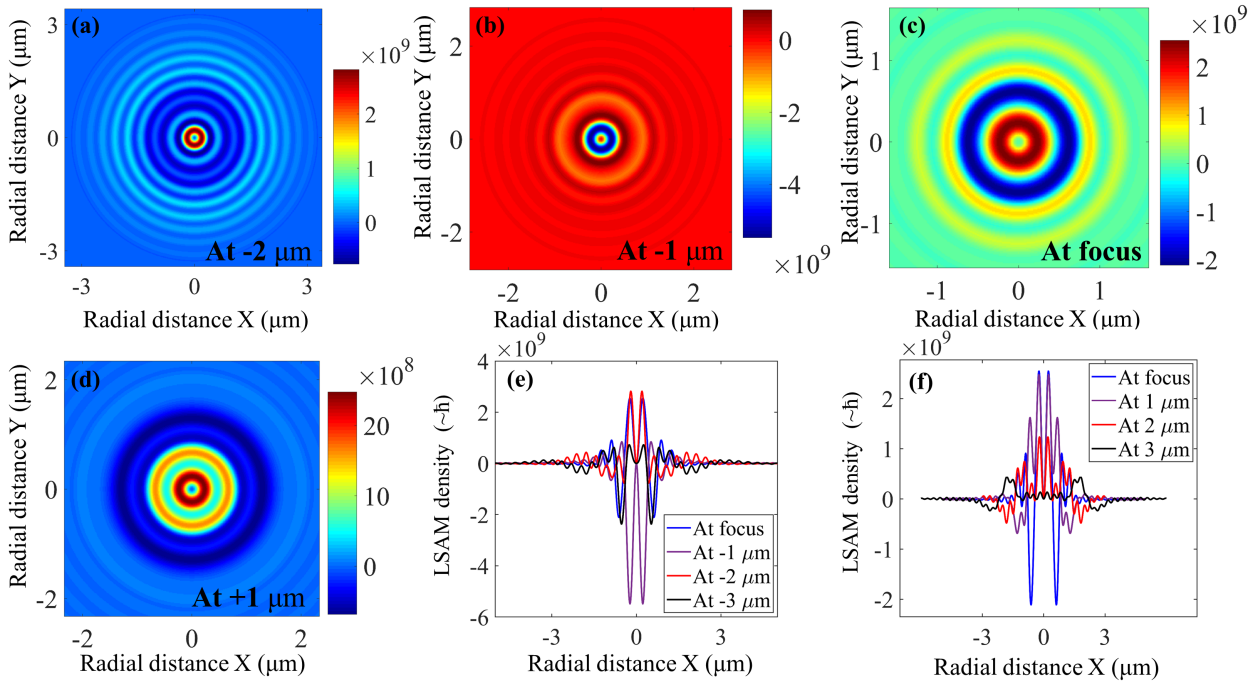

Fig 3 Numerical simulations of longitudinal spin angular momentum (LSAM) for an input anti-clockwise spirally polarized vector (ACW-SPV) beam before and after the focus of a high numerical aperture (NA) objective lens, with a refractive index (RI) of 1.814: (a) and (b) LSAM distributions at distances of $z = -2, \mu$m and $z = -1, \mu$m before the focus, respectively. (c) LSAM distribution at the focus. (d) LSAM distribution at a distance of $z = +1, \mu$m after the focus. (e) and (f) Comparisons of LSAM distributions before and after the focus, respectively, for the input ACW-SPV beam.

second annular rings of the LSAM correspond to the $\sigma = +1$ and $\sigma = -1$ helicities, respectively. Conversely, at $z = -1\,\mu$m and $z = -3\,\mu$m before the focus, the first and second annular rings of the LSAM correspond to the $\sigma = -1$ and $\sigma = +1$ helicities, respectively (see Fig. 3(e)). Therefore, a three-dimensional spin Hall effect exists before the focus, while the SHE is confined to the transverse plane after the focus.[11] Comparisons of LSAM distributions before and after the focus are shown in Figs. 3(e) and (f). It can be observed that the magnitude of LSAM (for both $\sigma = +1$ and $\sigma = -1$) is greater before the focus than after the focus. Furthermore, at the focal plane, the magnitudes of $\sigma = +1$ and $\sigma = -1$ are approximately equal. However, both before and after the focus (i.e., for negative and positive values of z), the magnitude of LSAM density near the beam center dominates over the off-axis LSAM density.

References

1 B. Richards and E. Wolf, "Electromagnetic diffraction in optical systems, ii. structure of the image field in an aplanatic system," *Proceedings of the Royal Society of London. Series A. Mathematical and Physical Sciences* **253**(1274), 358–379 (1959).

2 L. Novotny and B. Hecht, *Principles of Nano-optics*, Cambridge university press (2012).

3 B. Roy, N. Ghosh, S. D. Gupta, *et al.*, "Controlled transportation of mesoscopic particles by enhanced spin-orbit interaction of light in an optical trap," *Physical Review A* **87**(4), 043823 (2013).

4 Q. Zhan, "Cylindrical vector beams: from mathematical concepts to applications," *Advances in Optics and Photonics* **1**(1), 1–57 (2009).

5 D. L. Andrews and M. Babiker, *The angular momentum of light*, Cambridge University Press (2012).

6 R. N. Kumar, A. D. Ranjan, S. Roy, *et al.*, "Inhomogeneous-spin-momentum-induced orbital motion of birefringent particles in tight focusing of vector beams in optical tweezers," *Physical Review A* **110**(2), 023512 (2024).

7 R. N. Kumar, J. K. Nayak, S. D. Gupta, *et al.*, "Micromotors driven by spin-orbit interaction of light: Mimicking planetary motion at the microscale," *arXiv preprint arXiv:2410.20614* (2024).

8 E. Zauderer, "Complex argument hermite–gaussian and laguerre–gaussian beams," *JOSA A* **3**(4), 465–469 (1986).

9 S. D. Gupta, N. Ghosh, and A. Banerjee, *Wave optics: Basic concepts and contemporary trends*, CRC Press (2015).

10 R. N. Kumar, J. K. Nayak, S. D. Gupta, *et al.*, "Probing dual asymmetric transverse spin angular momentum in tightly focused vector beams in optical tweezers," *Laser & Photonics Reviews* **18**(2), 2300189 (2024).

11 W. Shu, C. Lin, J. Wu, *et al.*, "Three-dimensional spin hall effect of light in tight focusing," *Physical Review A* **101**(2), 023819 (2020).